Applied Catalysis B: Environmental 188 (2016) 272–282

Contents lists available at ScienceDirect

Applied Catalysis B: Environmental

journal homepage: www.elsevier.com/locate/apcatb

Gas phase electrocatalytic conversion of CO_2 to syn-fuels on Cu based catalysts-electrodes

N. Gutiérrez-Guerra [a], L. Moreno-López [a], J.C. Serrano-Ruiz [b], J.L. Valverde [a], A. de Lucas-Consuegra [a,*]

[a] Department of Chemical Engineering, School of Chemical Sciences and Technologies, University of Castilla-La Mancha, Avda. Camilo José Cela 12, 13005 Ciudad Real, Spain
[b] Abengoa Research, Abengoa, C/Energía Solar 1, Palmas Altas, 41014 Sevilla, Spain

ARTICLE INFO

Article history:
Received 22 September 2015
Received in revised form 1 February 2016
Accepted 3 February 2016
Available online 6 February 2016

Keywords:
CO_2 valorization
CO_2 electro-reduction
Cu catalyst
PEM
Energy vector

ABSTRACT

A novel electrocatalytic system based on a low temperature proton exchange membrane (Sterion) was developed for the gas phase electrocatalytic conversion of CO_2. This configuration allows the introduction of renewable energy in the chemical production chain via fuels production from direct CO_2 electro-reduction at atmospheric pressure and low temperatures (below 90 °C). For that purpose, three different Membrane Electrode Assemblies (MEAs) based on three different Cu based cathodic-catalysts were prepared and characterized: Cu-G/Sterion/IrO_2, Cu-AC/Sterion/IrO_2 and Cu-CNF/Sterion/IrO_2; graphite (G), activated carbon (AC) and carbon nanofibers (CNF). Thus, H_2O was fed and electrolyzed on the IrO_2 anode of the cell, thereby supplying H^+ across the membrane to react with CO_2 in the cathodic-catalyst and leading to the production of a mixture of syn-fuels (syn-gas, methanol, methane...). Remarkably, the nature of the cathodic-catalyst carbon support had a strong influence on the electrocatalytic activity and selectivity of the system. Hence, the Cu-AC-based cathodic-catalyst showed the highest CO_2 electrocatalytic activity, due to the highest surface area of the AC support and the larger metal dispersion of the Cu particles leading to acetaldehyde and methanol as the main reaction products. Besides the lower conductivity of the AC support, the lowest energy consumption values for CO_2 conversion and methanol and acetaldehyde production was also achieved with the MEA based on Cu-AC cathodic catalyst due to its higher electrocatalytic activity.

1. Introduction

The shift from a fossil fuel based economy towards a renewable energy one is a central strategy for achieving sustainability and energy efficiency in the chemical industry. In this regard, reducing CO_2 emissions is the key to proceed effectively in this direction. Two main technologies have been proposed so far: (i) capture and geological sequestration of CO_2 [1] and (ii) conversion into useful low-chain carbon fuels [2]. Sequestration still has certain barriers that make it unaffordable from an industrial point of view, such as the high cost of CO_2 capture, separation, purification and transportation. On the other hand, conversion into fuels seems to be a more attractive and promising solution that can meet the growing energy demands. The chemical conversion of CO_2 can be effectively performed via hydrogenation reactions [3–5]. This conversion can be achieved by chemical [6,7], photocatalytic [8], electrocatalytic [4,9–12], biological [13] and reforming [14] routes. Among them, the electrochemical pathway has been recognized as an efficient way to convert CO_2 to energy-rich products. The process possesses several advantages, namely: (i) control of the process by electrode potentials and reaction temperature; (ii) the supporting electrolytes can be fully recycled so that the overall chemical consumption can be minimized to simply water or wastewater; (iii) the electrochemical reaction systems are compact, modular, on-demand, and easy for scale-up applications; (iv) the electricity used to drive the process can be potentially obtained from a renewable source; (v) no external H_2 is required for the CO_2 reduction process as H^+ are in situ generated within the process. Hence, the valorization of the CO_2 molecule by electrochemical reduction has attracted worldwide interest due to its potential environmental and economic benefits [2,15–17]. This technology, when coupled to a renewable energy source such as solar and wind, could generate carbon neutral fuels or high added-value chemicals that are conventionally derived from petroleum at a competitive price. As a

* Corresponding author.
E-mail address: Antonio.lconsuegra@uclm.es (A. de Lucas-Consuegra).

http://dx.doi.org/10.1016/j.apcatb.2016.02.010
0926-3373/

matter of fact, the electrochemical reduction of CO_2 using a liquid electrolyte, either aqueous or organic, is being actively investigated in literature [18,19]. However, the main drawback of these processes is the recovery of the reaction product from the liquid electrolyte as the energy required to separate the products is higher than the energy stored in the produced molecules [10]. In this sense, the gas phase electrocatalytic conversion of CO_2 to liquid fuels allows easy product separation since there are no problems of solubility of CO_2 as in the case of liquid phase/electrolytes and no needs to recover the products from a liquid phase. Thus, gas-phase electroreduction of CO_2, mainly developed by the group of Prof. Centi [4,9–12], represents a valuable opportunity to incorporate renewable energy into the value chain of chemical industries. In this regard, the obtained products contain a higher energy density and are easier to transport and store. These previous studies have mainly used catalyst based on metal nanoparticles such as: Fe and Pt [4,9–12], Co [4] and Cu [4] supported over carbon nanotube (CNT) type materials. It has been shown that the nature of the nanocarbon substrate plays a relevant role in enhancing the productivity and tuning the selectivity towards c-chain products. However, the main disadvantage of this process is to control the localization of metal particles at the inner or outer surface of CNT which affects the obtained product distribution.

The gas phase electrocatalytic conversion of CO_2 is based on the use of a low temperature Proton Exchange Membrane (PEM) reactor configuration, consisting on a membrane electrode assembly (MEA) formed by an Anode/Membrane/Cathode system. Water is electrolyzed at the anode of the cell leading to the formation of O_2 and H^+ which are electrochemically supplied across the membrane to the cathodic-catalyst where they react with the adsorbed CO_2, leading to the formation of different molecules according to the following general reaction:

$$xCO_2 + 2(2x - z + y/2)H^+ + 2(2x - z + y/2)e^- \rightarrow C_xH_yO_z + (2x - z)H_2O \quad (1)$$

Hence, the influence of the cathodic-catalyst may have strong importance on the resultant electrocatalytic activity of the system.

In contrast to previous studies [4,9–12], this work reports for the first time a systematic study based on three different Cu cathodic-catalysts prepared on three different carbon supports: graphite (G), activated carbon (AC) and carbon nanofibers (CNF). The use of carbon materials has proven to be the best catalyst supports for such applications due to their specific properties, such as acid and base resistance, porosity, conductivity and the possibility of recovering the metals by combustion of the supports [20]. As a result, carbon materials have been used as conductive substrates for metal nanoparticles in electrocatalysis for the conversion of CO_2 [4,10,11]. The use of carbon-based electrocatalysts, e.g. similar to those used in PEM fuel cells, is critical to obtain good performances and control the selectivity in CO_2 conversion. In this sense, carbon support plays multiples roles in these types of systems by allowing a good dispersion of metal nanoparticles and especially facilitates the effectiveness of electrons and protons transport due to a better distribution of the metal nanoparticles [4]. On the other hand, copper was selected as catalyst due to its lower cost vs. other typically used materials. Additionally, a previous work [4] based on copper catalyst supported on carbon nanotubes showed its better performance among other materials for the electrocatalytic conversion of CO_2 to alcohols production under solventless conditions." Hence, in this work the role of different carbon supports as well as the influence of the applied current and reaction temperature on the catalytic activity and selectivity of the gas phase electrocatalytic conversion of CO_2 have been studied.

2. Experimental

2.1. Preparation of the Cu carbon supported cathodic catalysts

Copper catalysts supported on G, AC and functionalized CNF were used as cathode materials of the electrocatalytic reactor. Iridium (IV) oxide (IrO_2) was used as the anode.

Commercial graphite (Aldrich), commercial active carbon (Panreac) and synthesized functionalized carbon nanofibers were used as starting materials. Carbon nanofibers were prepared by the catalytic chemical vapor deposition method (CVD) in a fixed-bed reactor at atmospheric pressure. The synthesis was conducted over a Ni/SiO_2 (10%, w/w) catalyst at 600 °C to obtain fishbone type carbon nanofibers, employing ethylene as the carbon source and hydrogen as the carrier gas (C_2H_4/H_2, 4/1, v/v, 900 $Ncm^3\,min^{-1}$). The carbon deposit obtained was demineralized using HF (48%, v/v) in order to remove the parent catalyst particles and to avoid any residual Ni effect in later catalysts preparation/characterization steps. The material was dried for 12 h at 383 K in air to remove water prior to characterization. Further details regarding the CNF synthesis are given in a previous work [21]. The functionalization of the CNFs was performed by an oxidative treatment in HNO_3 to introduce oxygen functionalities on the carbon surface. Metal nanoparticles were later deposited on the graphite, active carbon and functionalized carbon nanofibers by the impregnation method. The different supports (G, AC and CNF) were placed in a glass vessel and kept under vacuum at room temperature for 2 h to remove water and other compounds adsorbed on the structure. A known volume of ethanolic solution of $Cu(NO_3)_2{\cdot}3H_2O$ (Panreac) (the minimum amount required to wet the solid) was then poured over the sample. After 2 h, the solvent was removed by evaporation under vacuum at 90 °C in a rotary evaporator. The catalysts were dried at 120 °C overnight, calcined in N_2 atmosphere at 350 °C using a heating ramp of 5 °C/min and kept at that temperature for 2 h. Finally, they were reduced in H_2 at 350 °C for 2 h (heating rate 5 °C min^{-1}). The total load of metal was around 50 wt.%.

2.2. Preparation of the electrodes and membrane electrode assembly (MEA)

The catalyst inks for the preparation of each electrode, anode and cathode respectively, were prepared by mixing appropriate amounts of the catalysts, IrO_2 commercial catalysts powders (Alfa Aesar, 99%), Cu-graphite powder, Cu-activated-carbon powder and Cu-carbon nanofibers powder with a Nafion solution (5 wt.%, Aldrich chemistry, Nafion® 117 solution) and isopropanol (Sigma Aldrich) with a binder/solvent volume ratio of 0.04. The selection of IrO_2 as the anode for the three explored MEAs has been done according to its unique and superior ability for water oxidation reaction in conventional PEM electrolyzers [22]. Then, the different inks were deposited on Carbon paper (Fuel Cell Earth) substrates at 65 °C until a metal loading of 0.5 mg cm^{-2} for each electrode was obtained after drying. The geometric surface area of both electrodes was 12.56 cm^2 (4 cm of circular diameter electrode). A proton conducting Sterion® membrane of 185 μm thickness (supplied by Hydrogen works) was used as the electrolyte (H^+ conductor material). Prior to use, the Sterion® membrane was treated by successive immersion at 100 °C for 2 h in H_2O_2 in order to remove organic impurities, in H_2SO_4 for activation and in deionized water to remove traces of solutions. Finally, in order to prepare the membrane electrode assembly (MEA), the membrane was sandwiched between the electrodes. Then, the whole system was hot-pressed using a press (GRASEBY SPEAC) at 120 °C and a pressure of 1 metric ton for 3 min.

2.3. Characterization of the Cu cathodic-catalysts and electrodes

The surface area/porosity measurements of the supports and powder catalysts were conducted using a Micromeritics ASAP 2010 for activated carbon and a QUADRASORB 3SI sorptometer apparatus for graphite and carbon nanofibers. In both cases, N_2 was used as the sorbate at −193 °C. The samples were outgased at 180 °C under vacuum (5×10^{-3} Torr) for 12 h prior to the analysis showing a slight weight loss due to the impurities, mainly wetness. Specific surface areas were determined by the multi-point BET method and Langmuir. The microporosity of the materials was evaluated by Howath-Kawazoe (HK) method and the mesoporosity was calculated by the Barret-Joyner-Halenda (BJH) method.

Cu metal loading, on the cathodic powdered catalyst was determined by atomic absorption spectrophotometry, using a SPECTRA 220FS analyzer. The sample (ca. 0.5 g) was treated in 2 mL HCl, 3 mL HF and 2 mL H_2O_2 followed by microwave digestion (T = 250 °C).

Temperature programmed reduction (TPR) experiments were also conducted for the different cathodic powder catalysts in a commercial Micromeritics AutoChem 2950HP unit equipped with a TCD detector. Samples (ca. 0.15 g) were loaded into a U-shaped tube and ramped from room temperature up to 900 °C (10 °C min^{-1}), using a reducing gas mixture of 17.5% v/v H_2/Ar (60 cm^3 min^{-1}).

Transmission electron microscopy (TEM) analyses for the powder cathodic-catalysts were conducted on a JEOL JEM-4000EX unit with an accelerating voltage of 400 kV. Samples were prepared by ultrasonic dispersion in acetone with a drop of the resulting suspension evaporated onto a holey carbon-supported grid.

Cu-based electrodes were also characterized before reaction tests by X-Ray Diffraction (XRD) analysis with a Philips PW-1710 instrument, using Ni-filtered Cu Kα radiation (λ = 1.5404 Å). The samples were scanned at a rate of 0.02°·$step^{-1}$ over the range $20° \leq 2\theta \leq 80°$ (scan time 2 s·$step^{-1}$) and the diffractograms were compared with the JCPDS-ICDD references

2.4. Catalytic activity measurements

The electrocatalytic experiments of CO_2 conversion were carried out in a lab-scale continuous electrocatalytic reactor operating at atmospheric pressure. Fig. 1 shows a schematic drawn of the electrocatalytic reactor. The cell reactor was made of two quartz tubes that act as cathodic and anodic compartments, and included two inlets, for CO_2 and H_2O/N_2, respectively, and two outlets streams. The system was heated with a furnace up to 90 °C connected to a K-type thermocouple and a temperature control system.

Water was introduced into the anode side of the cell by flowing N_2 through a saturator in order to achieve liquid/vapor equilibrium. The water content in the anodic chamber of reaction mixture (25% H_2O/N_2) was controlled by the vapor pressure of water at the temperature of the saturator (65 °C). All lines placed downstream from the saturator were heated above 100 °C to prevent condensation. In this side, the electrolysis of water was produced with the IrO_2 electrode in order to produce protons across the Sterion® membrane. Furthermore, the fed water stream was also used to hydrate the Sterion® membrane and keep its proton conductivity properties [4]. The cathodic part of the cell operates in contact with a gas flow of pure CO_2 (Praxair, Inc. certified standards 99.999% purity). Both gas flow rates (N_2 for the anode and CO_2 for the cathode) were controlled by a set of mass flowmeters (Brooks 5850 E and 5850 S).

The electrocatalytic experiments were carried out at atmospheric pressure with an overall gas flow rate of 0.5 NmL min^{-1} of CO_2 for the cathode (0.039 Nml min^{-1} cm^{-2}) and 6 NmL min^{-1} (0.47 Nml min^{-1} cm^{-2}) or the anodic stream (60% H_2O/N_2), at different temperatures (T = 80 °C and 90 °C, optimum values for the operation of the Sterion membrane). Reactants and products from the cathodic chamber of the cell were analyzed by using a double channel gas chromatograph (Bruker 450-GC) equipped with Hayesep and Q-Molsieve 13X consecutive columns and a CP-Wax 52CB column, along with thermal conductivity and flame ionization detectors, respectively. The detected products were CO_2, H_2, methane and CO for Hayesep and Q-Molsieve 13X columns and methanol, acetaldehyde, acetone, methyl formate, methyl acetate, ethanol, 2-propanol and *n*-propanol for CP-Wax 52CB column. The analytical limit of the analysis is bellow 1 ppm for each component. The detected reaction products were a mixture of syn-fuels: syn-gas (H_2, CO), CH_4, CO, methanol, acetaldehyde, acetone, methyl formate, ethanol, 2-propanol and *n*-propanol. The blank test carried out on a carbon paper support, feeding CO_2 in the cathode and H_2O in the anode did not show any electrocatalytic activity. The error in the carbon atom balance did not exceed 5%. A potentiostat/galvanostat (Voltalab 21, Radiometer Analytical) was used to supply a constant current (from −10 to −30 mA) between the electrodes which were connected using gold wires. The potentiostat-galvanostat was also used to perform voltammetry measurements under different reaction conditions.

The selectivity towards each compound was calculated by the following equation:

$$X_i\text{selectivity}/\% = \frac{F_{X_i}}{F^0_{CO_2}\text{-}F_{CO_2}} \text{x}100 \quad (2)$$

3. Results and discussion

3.1. Characterization of the Cu cathodic-catalysts and deposited electrodes

The three different cathodic-catalysts were characterized by N_2 adsorption, atomic absorption spectrophotometry, temperature-programmed reduction (TPR), transmission electron microscopy (TEM) and X-ray diffraction (XRD). Physicochemical properties of the supports, catalyst and fresh electrodes are shown in Table 1.

AC showed high values of Langmuir area and total pore volume, as previously described in literature [23] (Table 1). In this case, the N_2 adsorption/desorption isotherm (not shown) can be described as a combination of types I and IV isotherms (IUPAC classification) indicative of a microporous structure. Showing a narrow distributions of pore diameters with a mean value of 19 Å (Supplementary Fig. 1a), being close to the upper limit of the IUPAC accepted micropore range (<2 nm). On the other hand, graphite (G) was characterized by a low surface area and limited porosity showing a type IV adsorption/desorption isotherm (not shown), with a very small volume of adsorbed N_2 (Table 1). This fact is in good agreement with the low porosity of these materials [23]. The pore size distribution showed a narrow peak centered at 18 Å (Supplementary Fig. 1b). Finally, carbon nanofibers (CNF) showed a type IV N_2 adsorption/desorption isotherm (not shown). In this case, a mesoporous nature (2 nm < mesopore < 50 nm) was observed where the predominant pore size was 146 Å (Supplementary Fig. 1c) and a BET surface area in the range commonly observed for these materials was obtained (10–300 m^2 g^{-1}) [24] (Table 1). After the metal introduction, an important decrease of BET and Langmuir surface area and pore volume took place in all the cases which can be attributed to the partial pore blockage by metal particles [25].

This decrease is porcentually higher in the case of Cu/CNF (50% decrease vs 8% in the case of Cu/AC and 30% for Cu/G). Unlike AC and G supports, N_2 adsorption isotherm of CNF is characterized by a hysteresis loop (not shown) characteristic of mesoporous materials. Taking into consideration that Cu particles mean sizes lie right in the mesoporous range (40–96 nm), it seems logical that surface area decreases to a larger extent for that supports with a higher volume of mesoporous (Table 1). X-ray diffraction was used to study the graphitic character of the carbon materials. Interlayer spacing

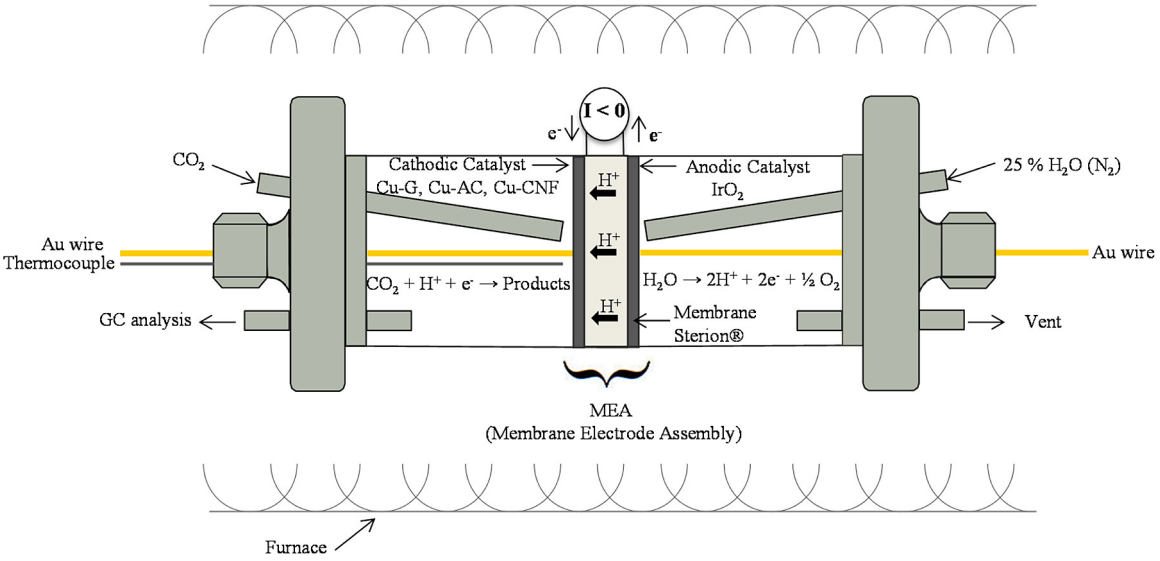

Fig. 1. Schematic drawn of the electrochemical reactor used for the CO_2 electrochemical conversion.

Table 1
Physicochemical properties of the supports, catalysts and fresh electrodes.

Sample	Surface area/$m^2\ g^{-1}$	Total pore volume/$cm^3\ g^{-1}$	Mesopore volume/$cm^3\ g^{-1}$	d_{002} (nm)	L_c (nm)	Powder metal loading/wt.%	TPR-T_{max}/°C	Particle size from TEM/nm
G	10	0.068	–	0.3364	32.21	–	–	–
Cu-G	7	0.046	0.046	–	–	51.46	198	96
AC	906	0.373	–	–	–	–	–	–
Cu-AC	836	0.211	0.100	–	–	53.97	207	40
CNF	95	0.555	–	0.3431	6.73	–	–	–
Cu-CNF	47	0.233	0.223	–	–	51.05	202	74

(d_{002}) and the average crystalline parameter (Lc) shown in Table 1, provided a measure of the structural order of the materials [20]. It increased with decreasing values of d_{002} and increasing values of Lc. Thus the structural order AC < CNF < G was obtained. First, activated carbon support, highly disorganized, did not exhibit any measurable graphiticity. On the other hand, graphite support showed the highest graphitic character. Finally, CNF support showed a moderate graphitic character. On the other hand, the total amount of Cu measured by the atomic absorption spectrophotometry was closed to 50% in three synthesized catalysts powders.

TPR profiles associated with each catalyst are given in Fig. 2. For the three catalysts the maximum reduction temperature was obtained at around 200 °C (T_{max}), which was characterized by a sharp peak. T_{max} obtained for each catalyst, associated with the first hydrogen consumption peak, are also given in Table 1. On other hand, an additional shoulder centered at around 250 °C was observed for the cathodic-catalysts Cu-G and Cu-AC [26]. This bimodal distribution of H_2-TPR was described by Kargol et al. [27]. The first temperature maximum is due to the reduction of CuO and partial reduction of Cu(II) ions to Cu(I). The presence of this compound has been proved by the XRD technique on the powder catalyst (not shown here). The second maximum corresponds to the reduction of Cu(I) or Cu (II) species strongly interacting with the support. On the other hand, the Cu-CNF cathodic-catalyst suggested one-step process of reduction. This process is ascribed to the direct reduction of CuO to metallic copper [27]. Finally, a third peak (appearing at temperature range between 520 and 600 °C) associated to the reduction of the oxygenated species was also observed for cathodic-catalyst Cu-CNF [24]. According to the obtained results, 350 °C was chosen as a suitable reduction temperature for each cathodic catalyst to ensure the metal activation without affecting the surface properties of the supports. Finally, the estimated hydrogen consumption as well as the percentage of the reducibility have been calculated. The Cu-AC catalyst showed the higher hydrogen consumption (5495 μmol g^{-1} cat) vs. the Cu-G and Cu-CNF (4202 μmol g^{-1} cat and 5495 μmol g^{-1} cat, respectively) due to the higher dispersion of Cu-AC, as shown later. In all cases, the copper has not been reduced completely. In this case, a relationship between the reducibility of copper (52% for Cu-G, 65% for Cu-AC and 58% for Cu-CNF) with the different used supports, the particle size and electrocatalytic activity has been obtained. The higher reducibility, the higher catalytic activity and lower particle size (as shown later).

Transmission electron microscopy (TEM) was used to determine the metal particle size and characteristics of the three prepared Cu-based cathodic-catalysts. Representative TEM micrographs are shown in Fig. 4 ((a) Cu-G powder, (b) Cu-AC powder and (c) Cu-CNF powder). In the present work, the mean Cu particle size, evaluated as the surface-are weighted diameter ($\bar{d}_s$) was calculated according to [28]:

$$\bar{d}_s = \frac{\sum_i n_i d_i^3}{n_i d_i^2} \quad (3)$$

where n_i represents the number of particles of diameter d_i.

The estimated particle size for the different catalyst is listed in Table 1. TEM micrographs for cathodic-catalysts, Cu-G (Fig. 3a) and Cu-CNF (Fig. 3c) showed a high particle size value (96 and 74 nm, respectively) and hence a lower dispersion of Cu particles is expected with respect to the Cu-AC powder. For this latter case (Fig. 3b), the corresponding TEM micrographs showed a smaller particle size (40 nm) and consequently, a higher dispersion of Cu particles on the AC support. This observation is related to the high

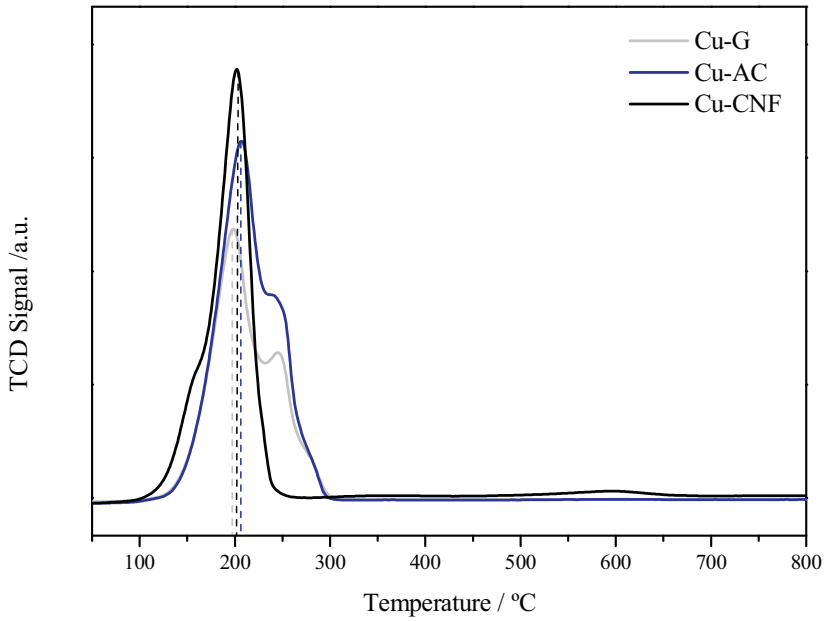

Fig. 2. TPR profiles of the fresh catalyst.

values of surface area and total pore volume obtained for the activated carbon support as discussed above. It is worth noting that for the case of cathodic-catalyst based on CNF (Fig. 3c), the carbon nanofibers can also be observed in the TEM images.

Fig. 4 shows the XRD analysis of the resultant Cu-based electrodes: Cu-G (a) Cu-AC (b) and Cu-CNF (c) (after deposition of the Cu cathodic-catalysts powders on the carbon paper substrates). The inset of Fig. 4a, b and c shows the magnification of XRD patterns. All samples showed two peaks around $2\theta = 25^\circ$ and 55°, which could be associated with the presence of the carbon paper substrate used as the current collector and gas diffusion layer. This fact was corroborated by the XRD spectrum of this material (not shown here). The main diffraction Cu peaks (1 1 1), (2 0 0), (2 2 0) and (3 3 1) appeared in the three cases at $2\theta = 43.3^\circ$, 50.4°, 74.1° and 90, respectively. These peaks are associated with metallic copper and exhibited a face-centered cubic (FCC) crystalline structure (JCPDS, 85–1326) (Inset of Fig. 4a, b and c). Additionally, the presence of small CuO peaks (1 1 1) and (2 2 3) could be detected at $2\theta = 32.5^\circ$ and 86.6°, respectively (JCPDS, 78-2076). However, the intensity of these peaks is very low which indicates that the copper is almost completely reduced and it has not been oxidized during the catalyst ink deposition on the carbon paper support. Additionally, no peaks related to the precursors were observed, which discards any contaminants coming from precursors.

Prior to the catalytic activity measurements, the three different MEAs (Cu-G/Sterion/IrO_2) (Fig. 5a), Cu-AC/Sterion/IrO_2 (Fig. 5b) and Cu-CNF/Sterion/IrO_2 (Fig. 5c) were in-situ characterized by a galvanostatic voltammetry under two different reaction atmospheres fed to the cathodic chamber: under presence of CO_2 ($F_{CO2,cathode} = 0.5\,NmL\,min^{-1}$, $F_{H2O,anode} = 6\,NmL\,min^{-1}$) and without feeding CO_2 to the cell ($F_{CO2,cathode} = 0\,NmL\,min^{-1}$, $F_{H2O,anode} = 6\,NmL\,min^{-1}$) at 90 °C. In this latter case, N_2 was fed to the cathodic side in order to purge the cell. The potential (U_{WC}) variation was recorded with the applied current (I) between 0 and −20 mA with a scan rate of 80 $\mu A\,s^{-1}$. It can be observed that for the three MEAs without feeding CO_2 to the cathode, water electrolysis began between −1.2 and −1.6 V [29], according to the following electrochemical reaction:

$$H_2O \rightarrow H^+ + \tfrac{1}{2}O_2 + e^- \quad (4)$$

An increase in the applied current led to higher negative potential values and hence to an increase in the protons production rate. At the cathodic side, hydrogen can be obtained due to the combination of protons that were transported through the protonic membrane and the electrons transferred from the external circuit:

$$2H^+ + 2e^- \rightarrow H_2 \quad (5)$$

On the other hand, it can be observed that for the three MEAs, a higher negative current values was obtained at fixed potential when CO_2 was fed to the cathode of the electrochemical system ($F_{CO2,cathode} = 0.5\,Nml\,min^{-1}/F_{H2O,anode} = 6\,Nml\,min^{-1}$). It demonstrates that the CO_2 present in the gas phase took part in the electrocatalytic process by its further adsorption and reaction on the cathodic-catalyst with the electrochemically supplied H^+. In fact the presence of CO_2 decreased the potential of the electrolysis cell (for the same current), then acting as a depolarizating agent for the electrochemical cathodic reaction (Reaction (1)) [30]. It demonstrates that CO_2 is adsorbed on the active cathodic catalyst and react with H^+ by the overall charge transfer Reaction (1) which may lead to the formation of different products as will be shown later. The use of different molecules as depolarizating agents has been studied for the electrolytic production of H_2 at high temperatures in Solid Oxide Electrolyzers. In this regard, the use of CH_4 [31,32], CO [33] and C [30,31] allowed to strongly decrease the required electrical power input for the electrolysis process via reaction with the O^{2-} ions transported across the Anionic Conductor Electrolyte. As can be observed in Fig. 5, the highest difference in the voltammetry experiments performed with and without CO_2 (highest depolarization effect) occurred with Cu-AC cathodic-catalyst. This fact can be attributed to the higher number of Cu active sites due to its higher dispersion on the high surface area AC support exposed to the gas phase. It probably facilitates the CO_2 adsorption leading to faster reaction kinetics with H^+, increasing the current at fixed potential. Then, one may expect a higher electrocatalytic activity of the cathodic-catalyst Cu-AC for the CO_2 electro-reduction (as will be shown later). Additionally, it can be observed that cathodic-catalyst Cu-AC achieved the higher potential range during voltammetry to reach the applied currents (up to −20 mA). It is due to the lower electrical conductivity (around $250\,\Omega^{-1}\,m^{-1}$) of the AC support vs. G and CNF which increase the overall electrical resistance of

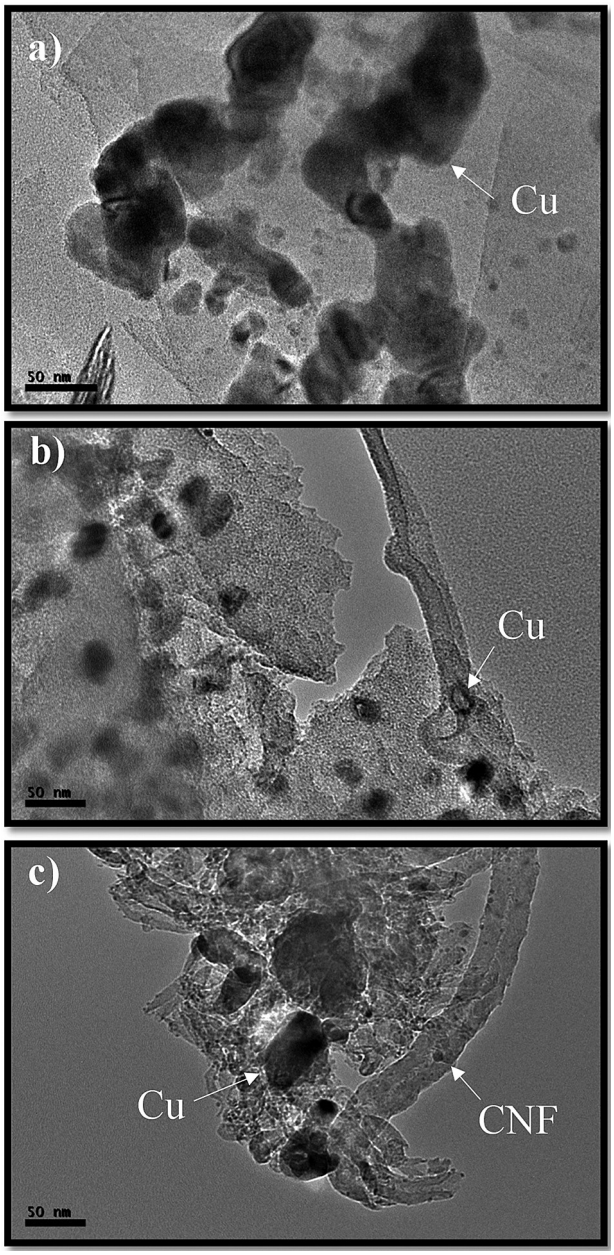

Fig. 3. Representative TEM images of the powders of (a) Cu-G, (b) Cu-AC and (c) Cu-CNF.

the MEA. Hence, the lowest potential range was obtained with cathodic-catalyst Cu-G, due to its highest electrical conductivity (around 1600 Ω^{-1} m^{-1}) among the carbonaceous supports. Finally, carbon nanofibers exhibited an intermediate electrical conductivity value (around 900 Ω^{-1} m^{-1}), leading to intermediate vales of the current-potential curves.

3.2. Electrocatalytic experiments for CO_2 conversion

Fig. 6 shows the time-on-stream evolution of the different measured products rates and the change in the potential as a function of time for a constant applied current of −20 mA at 90 °C for the three different cathodes under study at Temperature = 90 °C, $F_{CO2,cathode}$ = 0.5 NmL min^{-1}, $F_{H2O,anode}$ = 6 NmL min^{-1}. Initially, under open circuit conditions (O.C.C, no current application), no products were obtained at any case. Then, a constant current of −20 mA was applied for approximately 300 min under the same reaction atmosphere. During this current imposition step, hydrogen (not shown here via Reaction (5)), and different products such as methanol, acetaldehyde, acetone, methane, methyl formate, carbon monoxide, methyl acetate, ethanol, 2-propanol and *n*-propanol were obtained via CO_2 electro-reduction (Reactions (6)–(15). Most of these products have already been identified in similar previous studies of electrocatalytic conversion of CO_2 [4,9–12] using Fe, Co, Cu and Pt as cathodic-catalyst over CNT according to the following electrochemical reactions.

$$CO_2 + 6H^+ + 6e^- \rightarrow CH_3OH + H_2O \quad (6)$$

$$2CO_2 + 10H^+ + 10e^- \rightarrow CH_3CHO + 3H_2O \quad (7)$$

$$3CO_2 + 16H^+ + 16e^- \rightarrow CH_3COCH_3 + 5H_2O \quad (8)$$

$$CO_2 + 8H^+ + 8e^- \rightarrow CH_4 + 2H_2O \quad (9)$$

$$2CO_2 + 8H^+ + 8e^- \rightarrow HCOOCH_3 + 2H_2O \quad (10)$$

$$CO_2 + 2H^+ + 2e^- \rightarrow CO + H_2O \quad (11)$$

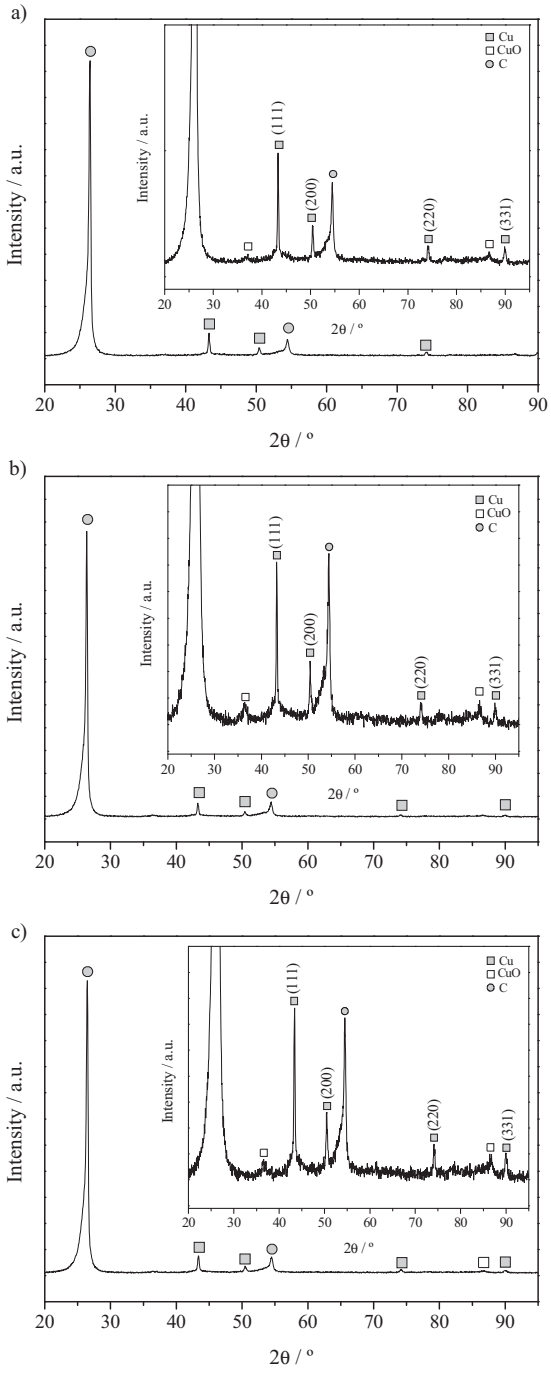

Fig. 4. XRD analysis patterns of cathodic-catalysts on carbon paper substrates: (a) Cu-G, (b) Cu-AC and (c) Cu-CNF. Insets in (a), (b) and (c) show the magnification of XRD patterns of cathodic-catalysts Cu-G, Cu-AC and Cu-CNF, respectively.

$$3CO_2 + 14H^+ + 14e^- \rightarrow CH_3COOCH_3 + 4H_2O \quad (12)$$

$$2CO_2 + 12H^+ + 12e^- \rightarrow CH_3CH_2OH + 3H_2O \quad (13)$$

$$3CO_2 + 18H^+ + 18e^- \rightarrow CH_3CH(OH)CH_3 + 5H_2O \quad (14)$$

$$3CO_2 + 18H^+ + 18e^- \rightarrow CH_3CH_2CH_2OH + 5H_2O \quad (15)$$

Finally, in all the experiments, the cathodic side of the cell was purged with N_2 (30 Nml min^{-1}) under open circuit conditions in order to remove all the products for subsequent reaction experiments.

In first place it should be mentioned that the electrochemical nature of the different obtained products vs. the catalytic route (CO_2 hydrogenation via previous H_2 evolution reaction) was confirmed with further experiments performed under open circuit conditions by co-feeding CO_2 and H_2 at the same temperature to the cathode (not shown here). Under these explored reaction conditions, no reaction products were detected confirming the electrochemical nature of the products observed on Fig. 6. It is further supported by the modification of the current-potential curves previously shown under presence of CO_2 during voltammetry experiments which confirms CO_2 adsorption and further reaction with H^+. This is in good agreement with previous works of catalytic CO_2 hydrogenation on Cu-based catalyst which showed that temperatures typically above 250 °C are required [34,35] for the process. The

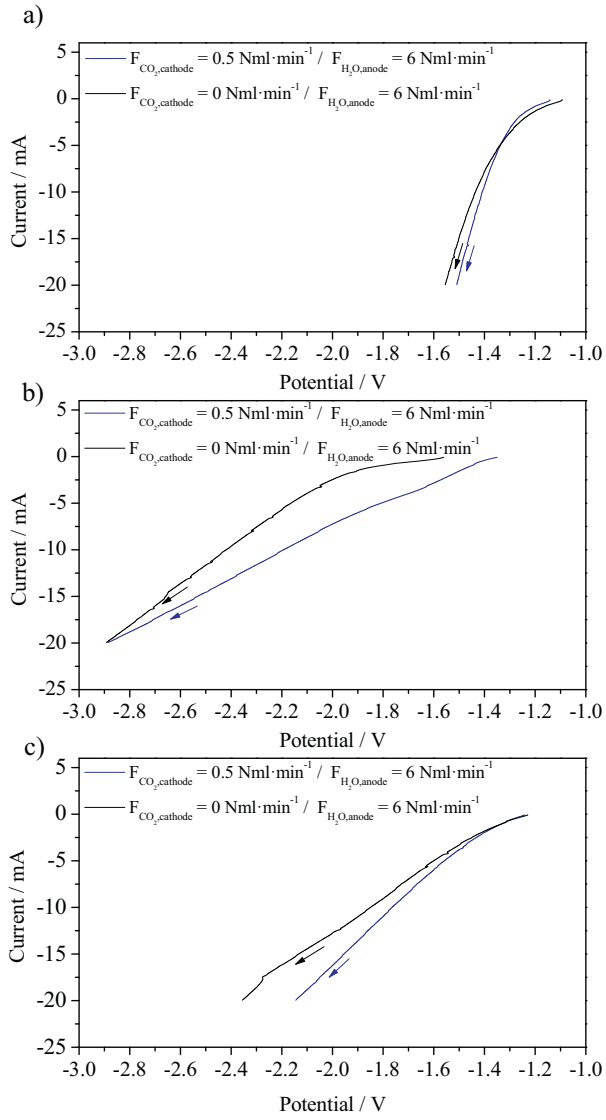

Fig. 5. Influence of the reaction atmosphere on the current-potential curves obtained during a galvanostatic voltammetry for cathodic-catalysts on carbon paper substrates: (a) Cu-G, (b) Cu-AC and (c) Cu-CNF. Conditions: temperature = 90 °C, sweep rate = 80 μA·s^{-1}.

coupling of the steam electrolysis process in the proposed configuration allows to directly supplying H^+ to the cathodic catalyst, of higher reactivity, which allows working at lower reaction temperatures vs. catalytic CO_2 hydrogenation processes.

On the other hand it can be observed that among the three investigated cathodic-catalyst, the Cu-AC system showed the higher electrocatalytic activity (around five times higher) in comparison with the other two cathodic-catalysts: Cu-G and Cu-CNF. This observation is in good agreement with the galvanostatic voltammetry curves previously shown which demonstrates the higher depolarization effect caused by CO_2 on the MEA based on Cu-AC. This higher electrocatalytic activity could be related to the higher surface area and the higher porosity of the C support leading to a higher metal dispersion of the Cu particles, which is a key factor for CO_2 adsorption and further reaction via the electrochemical Reactions (6)–(10). It should be mentioned that on these experiments the effect of the conductivity of the different carbon supports it is not affecting the electrocatalytic activity of the system since the three MEAS are compared under the same current application (−20 mA), i.e., under the same H^+ supplied rate to the cathode ($r = I/(nF) = 1.036 \cdot 10^{-7}$ mol s^{-1}). However, is clear that a high potential will be required to achieve the current of −20 mA for the case of the Cu-AC cathodic catalyst (−2.72 V) vs. the Cu-G and Cu-CNF (−1.54 V and −2.11 V respectively), therefore leading to a higher electrical energy consumption. In all cases, it can be observed the stability of the potential obtained during long periods of reaction confirming the stability of the different electrodes under polarization conditions.

Concerning the different obtained products it can be observed that methanol was the main reaction product for the case of the Cu-G cathodic-catalyst while acetaldehyde was the main one for the case of Cu-AC and Cu-CNF systems. This observation can be explained according to previous studies of catalytic CO_2 hydrogenation that have shown that Cu particles of higher size are more selective for methanol production rather than for acetaldehyde [36,37]. On the other it should be mentioned that a wider variety of reaction products with higher number of carbon atoms was obtained for the case of Cu-CNF cathodic-catalyst, which could be related to the presence of the functional oxygen groups in the CNF support. As reported by Genovese et al. [4], the nature of functional groups on the carbon surface when CNF is used as a catalyst support

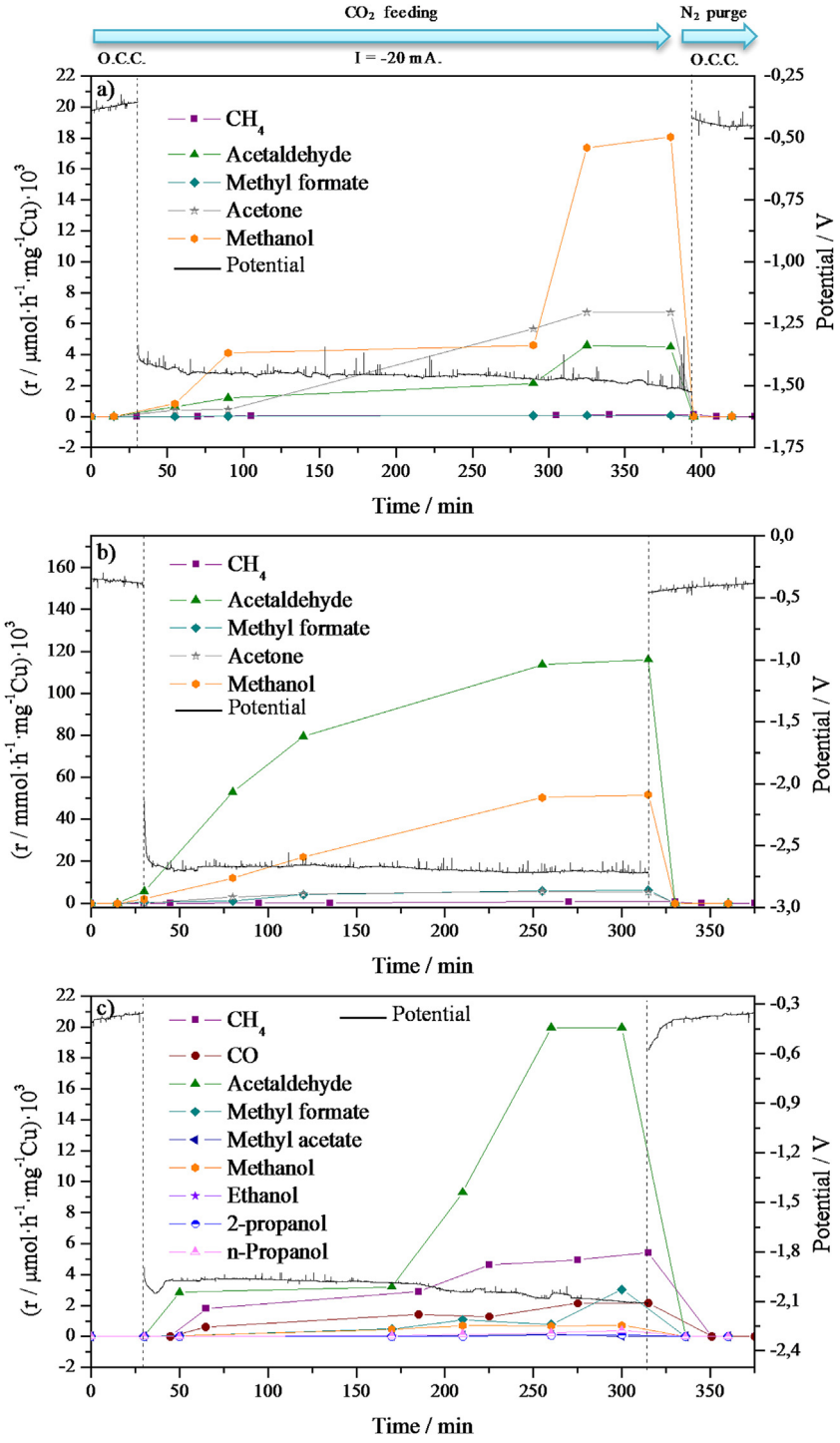

Fig. 6. Time-on-stream variation of different products and potential for a constant current of −20 mA. Cathodic-catalysts on carbon paper substrates: (a) Cu-G, (b) Cu-AC and (c) Cu-CNF. Conditions: temperature = 90 °C, $F_{CO2,cathode}$ = 0.5 NmL·min^{-1}, $F_{H2O,anode}$ = 6 NmL min^{-1}.

has a significant influence on determining the possibility to form >C_1 products from CO_2.

Fig. 7a and b shows the effect of the applied current and reaction temperature, respectively, in the normalized CO_2 electrocatalytic steady state reaction rate (per mg of deposited Cu) after 300 min of polarization at each current. In agreement with the previous experiment, it can be observed that for all the explored reaction conditions (applied currents and temperatures), the electrocatalytic activity of the cathodic-catalyst Cu-AC is higher than that of Cu-G and Cu-CNF. Additionally, it can be observed that the higher the applied current, the higher the CO_2 reaction rate, attributed to the higher amount of H^+ ions electrochemically supplied. On the other hand, the higher the reaction temperature, the higher the electrocatalytic activity of the system. This fact can be attributed to the enhanced kinetics of electrochemical reactions at higher reaction temperature [38]. However, 90 °C was the highest explored temperature, which ensures the stability and conductivity of the protonic membrane under suitable humidity conditions.

The influence of the applied current (I = −10, −20 and −30 mA) on the steady state variation of the selectivity of the different prod-

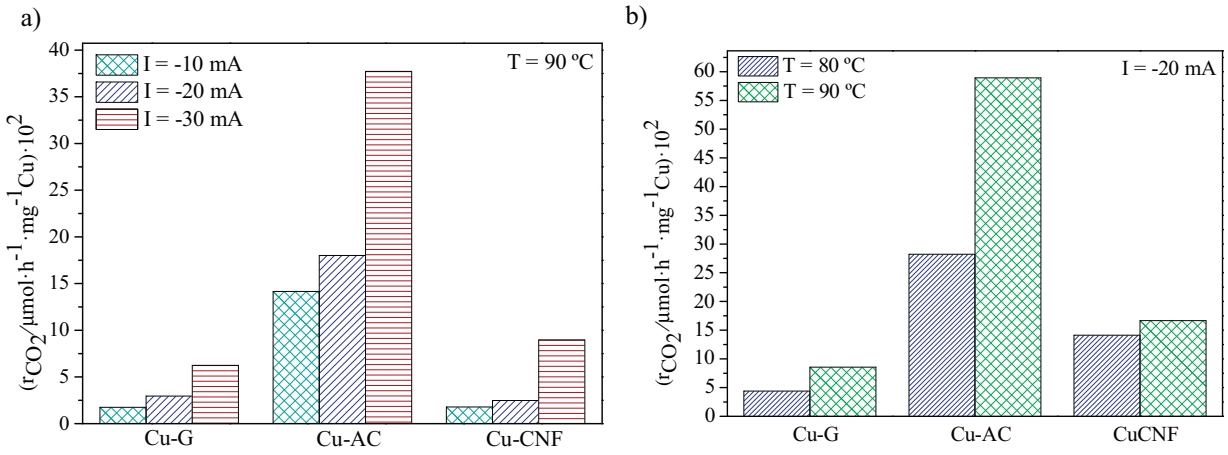

Fig. 7. (a) Effect of the current at 90 °C and (b) temperature (T = 80 and 90 °C) at I = −20 mA on the steady state CO_2 consumption rate for Cu/Sterion/IrO_2 and Cu-C/Sterion/IrO_2 electrodes. Conditions: $F_{CO2,cathode}$ = 0.5 NmL min^{-1}, $F_{H2O,anode}$ = 6 NmL min^{-1}.

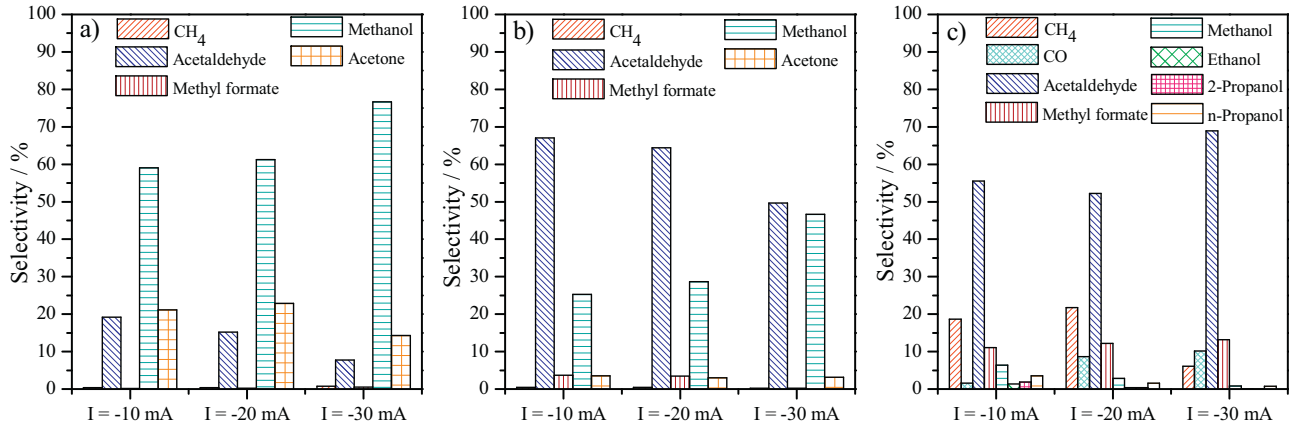

Fig. 8. Effect of the applied current on the steady state selectivity toward the different products on Cu cathodic-catalysts: (a) Cu-G, (b) Cu-AC and (c) Cu-CNF. Conditions: Temperature = 90 °C, $F_{CO2,cathode}$ = 0.5 NmL min^{-1}, $F_{H2O,anode}$ = 6 NmL min^{-1}.

ucts was studied at 90 °C (Fig. 8) after the polarization at each current for 300 min: for cathodic-catalysts Cu-G, Cu-AC and Cu-CNF, Fig. 8a–c, respectively. As shown before, methanol was the main obtained product on cathodic-catalyst Cu-G. In this case, the selectivity to methanol varied between 60% under I = −10 mA and 75% for an applied current of I = −30 mA. On the other hand, for the cathodic-catalysts Cu-AC and Cu-CNF, acetaldehyde was the main reaction product with selectivity values around 60%. It can be observed that for the case of Cu-G and Cu-AC (Fig. 8a and b) an increase in the applied cathodic current (from −10 mA to −30 mA) led to an increase in the methanol selectivity at the expense of a decrease in the acetaldehyde. In this case is clear that at higher supplied rate of protons at higher intensity values the selectivity shift to lighter and more saturated compounds in agreement with previous studies [39,40], i.e. toward methanol production (Reaction (6)). However, for the Cu-CNF cathodic-catalyst, the variation of product selectivity with the applied current does not seem to follow a clear trend, probably due to the high number of obtained products obtained and to the complex number of reactions that occurred on the system.

In order to finally address, the best electrocatalytic system in terms of activity but also energy consumption, Table 2 shows a comparison between the three different MEAs at T = 90 °C and I = −30 mA for the overall energy consumption for CO_2 conversion (kWh mol$^{-}{}_{CO2}$) as well as energy consumption for the production of methanol (kWh mol$^{-}{}_{CH3OH}$) and acetaldehyde (kWh mol$^{-}{}_{CH3CHO}$). Even though, the AC support has the lower electrical conductivity value (as shown on the voltammetry curves of Fig. 5) its higher activity at the same current conditions shown on Figs. 6 and 7 led to the lower energy consumption values for CO_2 conversion and methanol and acetaldehyde production. Hence, the MEA based on the Cu-AC cathodic-catalyst consumed less energy per kg of methanol produced and per kg of acetaldehyde produced than the other two MEAs based on Cu-G and Cu-CNF cathodic-catalyst. In addition the MEA based on Cu-AC cathodic catalysts allows to obtained liquid fuels at room pressure and low temperature such as: methanol and acetaldehyde with an overall selectivity above 90% (Fig. 8b) which can be then easily separated from gaseous CO_2. For each system the lower energy consumption is evidently obtained with the most selective product: methanol for the case of Cu-G cathodic catalyst and acetaldehyde for the case of Cu-AC and Cu-CNF. These results allow to conclude that among the three different explored cathodic catalyst, the higher activity of the Cu-AC cathodic catalyst due to the higher disper-

Table 2
Comparison of the energy consumption for the three different Cu based cathodic catalyst in the electrocatalytic conversion of CO_2 at 90 °C and I = −30 mA.

Sample	kWh mol$^{-1}{}_{CO2}$	kWh mol$^{-1}{}_{CH3OH}$	kWh mol$^{-1}{}_{CH3CHO}$
Cu-G	199.8	260.6	2574.7
Cu-AC	92.4	197.9	185.9
Cu-CNF	189.1	23785.5	274.2

sion of Cu particles on the high surface area AC support is the most important parameter besides its lower electrical conductivity. However, is clear that suitable values of both parameters: activity and conductivity should be found for the design of efficient cathodic catalyst for the CO_2 electrochemical conversion. Then the use of novel supports (e.g. reduced graphene powder, carbon black, molybdenum-carbide-derived carbon. . .) of high surface area and high electrical conductivity may decrease the overall energy consumption values reported on Table 2 in view of the practical application of this configuration for the renewable production of solar fuels via electrochemical conversion of CO_2.

4. Conclusions

Three different Cu-based cathodic-catalysts (metal loading closed to 50%) supported on Graphite (G), Activated Carbon (AC) and Carbon Nanofibers (CNF) have been prepared via impregnation technique and characterized by different techniques.

Among them, the Cu-AC-based cathodic-catalyst showed the highest CO_2 electrocatalytic activity under all the explored reaction conditions, due to the highest surface area of the AC support and the larger metal dispersion of the Cu particles. Methanol was the main reaction product for the case of the Cu-G cathodic-catalyst while acetaldehyde was the main one for the case of Cu-AC and Cu-CNF systems which can be attributed to the higher size of Cu particle sizes in these two latter cases.

Concerning the product selectivity variation with the current, for the cased of Cu-G and Cu-AC cathodic catalyst, an increase in the applied cathodic current led to an increase in the methanol selectivity at the expense of a decrease in the acetaldehyde one. In this case is clear that at higher supplied rate of protons at higher intensity values the selectivity shift to lighter and more saturated compounds. However, for the Cu-CNF cathodic-catalyst, the variation of product selectivity with the applied current does not seem to follow a clear trend, probably due to the high number of obtained products obtained and to the complex number of reactions that occurred on the system.

Besides the lower conductivity of the AC support, the lowest energy consumption values for CO_2 conversion and methanol and acetaldehyde production was achieved with the MEA based on Cu-AC cathodic catalyst. Therefore, the higher activity of the Cu-AC cathodic catalyst due to the higher dispersion of Cu particles on the high surface area AC support is the most important parameter besides its lower electrical conductivity.

Appendix A. Supplementary data

Supplementary data associated with this article can be found, in the online version, at http://dx.doi.org/10.1016/j.apcatb.2016.02.010.

References

[1] C. Rodrigues, M. Dinis, M. Lemos de Sousa, Environ. Earth Sci. 74 (2015) 2553–2561.
[2] J. Qiao, Y. Liu, F. Hong, J. Zhang, Chem. Soc. Rev. 43 (2014) 631–675.
[3] D. Theleritis, S. Souentie, A. Siokou, A. Katsaounis, C.G. Vayenas, ACS Catal. 2 (2012) 770–780.
[4] C. Genovese, C. Ampelli, S. Perathoner, G. Centi, J. Catal. 308 (2013) 237–249.
[5] W. Wang, S. Wang, X. Ma, J. Gong, Chem. Soc. Rev. 40 (2011) 3703–3727.
[6] W. Leitner, Angew. Chem. Int. Ed. Engl. 34 (1995) 2207.
[7] I. Omae, Coord. Chem. Rev. 256 (2012) 1384–1405.
[8] K. Mori, H. Yamashita, M. Anpo, RSC Adv. 2 (2012) 3165–3172.
[9] C. Genovese, C. Ampelli, S. Perathoner, G. Centi, Chem. Eng. Trans. 11 (2013) 289–294.
[10] C. Genovese, C. Ampelli, S. Perathoner, G. Centi, J. Energ. Chem. 22 (2013) 202–213.
[11] M. Gangeri, S. Perathoner, S. Caudo, G. Centi, J. Amadou, D. Bégin, C. Pham-Huu, M.J. Ledoux, J.P. Tessonnier, D.S. Su, R. Schlögl, Catal. Today. 143 (2009) 57–63.
[12] G. Centi, S. Perathoner, G. Wine, M. Gangeri, Green Chem. 9 (2007) 671–678.
[13] C. Stewart, M.-A. Hessami, Energy Convers. Manag. 46 (2005) 403–420.
[14] V.R. Choudhary, A.M. Rajput, B. Prabhakar, Catal. Lett. 32 (1995) 391–396.
[15] J. Albo, M. Alvarez-Guerra, P. Castano, A. Irabien, Green Chem. 17 (2015) 2304–2324.
[16] S. Saeidi, N.A.S. Amin, M.R. Rahimpour, J. CO_2 Util. 5 (2014) 66–81.
[17] G. Centi, E.A. Quadrelli, S. Perathoner, Energy Environ. Sci. 6 (2013) 1711–1731.
[18] J. Ma, N. Sun, X. Zhang, N. Zhao, F. Xiao, W. Wei, Y. Sun, Catal. Today 148 (2009) 221–231.
[19] Y. Hori, I. kahashi, O. Koga, N. Hoshi, J. Mol. Catal A: Chem. 199 (2003) 39.
[20] S. Gil, L. Muñoz, L. Sánchez-Silva, A. Romero, J.L. Valverde, Chem. Eng. J. 172 (2011) 418–429.
[21] V. Jiménez, A. Nieto-Márquez, J.A. Díaz, R. Romero, P. Sánchez, J.L. Valverde, A. Romero, Ind. Eng. Chem. Res. 48 (2009) 8407–8417.
[22] J.C. Tokash, B.E. Logan, Int. J. Hydrogen Energy 36 (2011) 9439–9445.
[23] F. Rodríguez-reinoso, Carbon 36 (1998) 159–175.
[24] J.A. Díaz, M. Martínez-Fernández, A. Romero, J.L. Valverde, Fuel 111 (2013) 422–429.
[25] M. Molina-Sabio, V. Pérez, F. Rodríguez-Reinoso, Carbon 32 (1994) 1259–1265.
[26] C. Huo, J. Ouyang, H. Yang, Sci. Rep. 4 (2014) 3682–3691.
[27] M. Kargol, J. Zajac, D.J. Jones, J. Rozière, T. Steriotis, A. Jiménez-López, E. Rodríguez-Castellón, Chem. Mater. 17 (2005) 6117–6127.
[28] J.M. García-Vargas, J.L. Valverde, F. Dorado, P. Sánchez, J. Mol. Catal. A: Chem. 395 (2014) 108–116.
[29] B. Lee, K. Park, H.M. Kim, Int. J. Electrochem. Sci. 8 (2013) 235–248.
[30] A.C. Lee, R.E. Mitchell, T.M. Gür, Solid State Ionics 192 (2011) 607–610.
[31] A. de Lucas-Consuegra, N. Gutiérrez-Guerra, A. Caravaca, J.C. Serrano-Ruiz, J.L. Valverde, Appl. Catal. A 483 (2014) 25–30.
[32] J. Martinez-Frias, A.-Q. Pham, S.M. Aceves, Int. J. Hydrogen Energy 28 (2003) 483–490.
[33] W. Wang, J. Vohs, R. Gorte, Top. Catal. 46 (2007) 380–385.
[34] H. Ahouari, A. Soualah, A. Le Valant, L. Pinard, P. Magnoux, Y. Pouilloux, React. Kinet. Mech. Cat. 110 (2013) 131–145.
[35] S.-i. Fujita, M. Usui, E. Ohara, N. Takezawa, Catal. Lett. 13 (1992) 349–358.
[36] A. Karelovic, P. Ruiz, Catal. Sci. Technol. 5 (2015) 869–881.
[37] F. Arena, K. Barbera, G. Italiano, G. Bonura, L. Spadaro, F. Frusteri, J. Catal. 249 (2007) 185–194.
[38] A. Caravaca, F.M. Sapountzi, A. de Lucas-Consuegra, C. Molina-Mora, F. Dorado, J.L. Valverde, Int. J. Hydrogen Energy 37 (2012) 9504–9513.
[39] V.R. Rao Pendyala, G. Jacobs, J.C. Mohandas, M. Luo, W. Ma, M.K. Gnanamani, B.H. Davis, Appl. Catal. A 389 (2010) 131–139.
[40] M.E. Dry, Catal. Today 71 (2002) 227–241.